PAPER

PCA-Based Retinal Vessel Tortuosity Quantification

Rashmi TURIOR[†a)], ***Student Member***, **Danu ONKAEW**[†b)], ***and*** **Bunyarit UYYANONVARA**[†c)], ***Nonmembers***

SUMMARY Automatic vessel tortuosity measures are crucial for many applications related to retinal diseases such as those due to retinopathy of prematurity (ROP), hypertension, stroke, diabetes and cardiovascular diseases. An automatic evaluation and quantification of retinal vascular tortuosity would help in the early detection of such retinopathies and other systemic diseases. In this paper, we propose a novel tortuosity index based on principal component analysis. The index is compared with three existant indices using simulated curves and real retinal images to demonstrate that it is a valid indicator of tortuosity. The proposed index satisfies all the tortuosity properties such as invariance to translation, rotation and scaling and also the modulation properties. It is capable of differentiating the tortuosity of structures that visually appear to be different in tortuosity and shapes. The proposed index can automatically classify the image as tortuous or non tortuous. For an optimal set of training parameters, the prediction accuracy is as high as 82.94% and 86.6% on 45 retinal images at segment level and image level, respectively. The test results are verified against the judgement of two expert Ophthalmologists. The proposed index is marked by its inherent simplicity and computational attractiveness, and produces the expected estimate, irrespective of the segmentation approach. Examples and experimental results demonstrate the fitness and effectiveness of the proposed technique for both simulated curves and retinal images.

key words: *tortuosity, retinopathy of prematurity (ROP), principal component analysis*

1. Introduction

Tortuosity evaluation is a crucial task in many applications pertaining to retinal diseases such as those due to retinopathy of prematurity (ROP). ROP is a disease affecting infants, characterized by an increase in vascular dilation and tortuosity. Tortuosity is defined as non-smooth appearance of vessel course. Deformation in the blood vessel network of the retina are indicators of not only retinal pathologies but also other systemic diseases coming from cardiovascular, central nervous and endocrine-metabolic systems [1]. Tortuosity is known to track Plus disease, one of the most important prognostic indicators in ROP, better than dilation [2].

Tortuosity definition in clinical terms is still unclear and thus a standard needs to be set in this field. In clinical practice ophthalmologists commonly grade tortuosity using a qualitative scale (e.g. mild, moderate, severe and extreme) [3], but a reliable quantitative measure would enable the automated measurement of retinal vascular tortuosity and its progression to be more easily discerned. Many techniques have been devised to classify tortuosity, but relatively few attempts have been made to quantify it. W. Lotmar et al. and Bracher et al. proposed tortuosity measure based on the ratio of arc length and chord length [4], [5]. However, it was recognised as flawed [2] since a vessel that bends gradually can yield the same numeric value as the one that bends more frequently. The authors in [6] formulated automated measurement using seven integral estimates of tortuosity based on the curvature of vessels. However, it failed in differentiating the tortuosity of structures that visually appear to be different in tortuosity. For better accuracy of tortuosity calculation, Bullitt et al. [7] generalized Harts estimates to 3D images obtained by means of the Magnetic Resonance Angiography. Measurement of tortuosity using relative length variation was proposed by Kylstra et al. [8]. His study indicates relationships between tortuosity, diameter and pressure that affect the change in the shape of artificial latex vessels. In [9], the authors intended to measure tortuosity by using Fourier analysis. Dougherty and Varro [10] calculated the tortuosity using second derivatives along central axis of the blood vessels. Gao et al. [11] developed an interface based on MIDAS, but it proved to be subjective and time consuming.

Pederson et al. [12] proposed to measure vessel diameter using two different methods to estimate profile width, but in this case bifurcations and crossings were not considered while choosing the vessel segment. E. Grisan et al. [13] proposed an alternative method based on partitioning of the blood vessels into segments called turn curves, and calculated tortuosity of each individual segment. The idea behind this is to use the points of changing curvature sign. However, this algorithm required manual vessel extraction and inflection point placement. Heneghan et al. [14] and Sukkaew et al. [15] applied the method called Arc length over Chord length ratio, which used the length of a straight line over considered part of the vessel. But this method required proper partitioning values for each part of the blood vessel to avoid significant error. Estimates based on curve partitioning often proved as flawed in many cases such as, a circle arc with a large radius is non-tortuous although the ratio between arc length and chord length could be very large. Johnson et al. defined robust metrics employing unit speed parameterization for quantifying vascular tortuosity in terms of 3-D curvature [16].

We propose a new tortuosity measure that circumvents the limitations posed by the previous available indices. This

Manuscript received April 23, 2012.
Manuscript revised October 8, 2012.

[†]The authors are with the Sirindhorn International Institute of Technology, Thammasat University, Thailand.
a) E-mail: rashmi.turior@siit.tu.ac.th
b) E-mail: danu.onkaew@siit.tu.ac.th
c) E-mail: bunyarit@siit.tu.ac.th

DOI: 10.1587/transinf.E96.D.329

paper proposes a novel tortuosity index, and compares it with three existant indices using simulated curves and real retinal images to demonstrate that it is a valid indicator of tortuosity. The paper is outlined as follows. Section 2 describes the abstract properties of a valid tortuosity index and provides an overview of the available indices and the proposed methodology. Section 3 shows the results and evaluation of the algorithm on simulated shapes and real blood vessels, followed by discussions and conclusions in Sect. 4

2. Methods

2.1 Abstract Tortuosity Properties

There is no formal clinical definition of vessel tortuosity measures; however there are some intuitive notions of tortuosity, which a reasonable index must satisfy. A valid tortuosity metric should work as a prognostic indicator of the ophthalmologists' notion of tortuosity. Therefore, it becomes imperative to discuss the properties of tortuosity measures.

2.1.1 Invariance to Translation, Rotation and Scaling

Translation and rotation transformations do not influence the perception of tortuosity as they are related to the topology and orientation of the vessels in a retina and consequently do not alter in any way the clinical evaluation of tortuosity. Ophthalmologists have equivocal intuitions of another one property as invariance to scaling or independence of linear scaling. The value of the index should be independent of magnification of the image of a vessel. However, if a tortuosity metric does vary with change in scale, it does so in multiples.

2.1.2 Compositionality Property

The property of compositionality is concerned with the manner in which the tortuosity of a vessel, comprising several segments is computed. For example, given two continuous curves c_1 and c_2, as part of the same vessel, the combination of the two is defined as

$$c_3 = c_1 + c_2$$

maintaining the continuity of c_3 since the two constituent curves belong to the same vessel.

According to the intuitive empirical principle proposed [6] for the tortuosity, Γ of two curves c_1 and c_2

$$\Gamma(c_1) \leq \Gamma(c_2) \Rightarrow \Gamma(c_1) \leq \Gamma(c_1 + c_2) \leq \Gamma(c_2) \quad (1)$$

This implies the resulting tortuosity is between those of the two composing curve. The method proposed in [6] was referred as weighted additive expressed as,

$$\Gamma(c_1 + c_2) = [\Gamma(c_1)L(c_1) + \Gamma(c_2)L(c_2)]/L(c_1 + c_2) \quad (2)$$

where $L(c)$ is the arc length of the curve, c. However, this notion is contradicted with the principle of invariance with respect to rotation and scale, since tortuosity of the vessel cannot be less than any of its constituent segments. Therefore, a composition property indicating full compliance with the additive property was proposed [13], such that a vessel curve c, combination of several segments c_i, was given by adding together the tortuosity values of its constituent segments that is,

$$\Gamma(c_i) \leq \Gamma(c_1 + c_2 + \ldots\ldots + c_n) \quad (3)$$

where i varies from 1 to n and c_i is a subset of the parent vessel, c. However, computation of tortuosity of a vessel depend on whether the comprising segments belong to the same vessel, as a result averaging the tortuosity of its constituent segments to evaluate the net tortuosity of the parent vessel does not hold true. In the proposed method, estimation of tortuosity is done on sub vessel samples (a subsegment of the vessel tree enclosed by a branch point and an end point or two end points). Hence it is concluded that, our measure of evaluating tortuosity of a vessel is independent of vessel sub segmentation and the tortuosity of the segments comprising the sub vessel samples. In the present work, the vessel tree is partitioned into sub vessels and net tortuosity of the entire vessel tree is computed by taking the mean of sum of the tortuosity of each sub vessel samples in the blood vessel network.

2.1.3 Modulation

To assess the appearance of the blood vessel and its behavior under varied circumstances, the property of modulation holds immense importance. It is expressed in two forms: change in frequency referred as frequency modulation at fixed amplitude and change in amplitude referred as amplitude modulation at fixed frequency. It may be assumed that the greater number of changes in curvature sign (twist), the greater the tortuosity associated with it will be. Likewise, the higher the amplitude of a twist, (as defined in [13]) the more tortuous, the vessel will be considered.

$$N(c_1) \leq N(c_2) \Rightarrow \Gamma(c_1) \leq \Gamma(c_2) \quad (4)$$

$$A(c_1) \leq A(c_2) \Rightarrow \Gamma(c_1) \leq \Gamma(c_2) \quad (5)$$

Where N is the number of twists and A is the amplitude of the twists.

2.2 Available Tortuosity Measures

Various tortuosity measures have been proposed in literature but all pose certain constraints, thereby restricting its application. In this section we review two such measures for evaluating retinal vessel tortuosity and demonstrate their shortcomings as compared to the proposed index.

2.2.1 Arc Length over Chord Length Ratio

The simpler and the most widely used measure of tortuosity

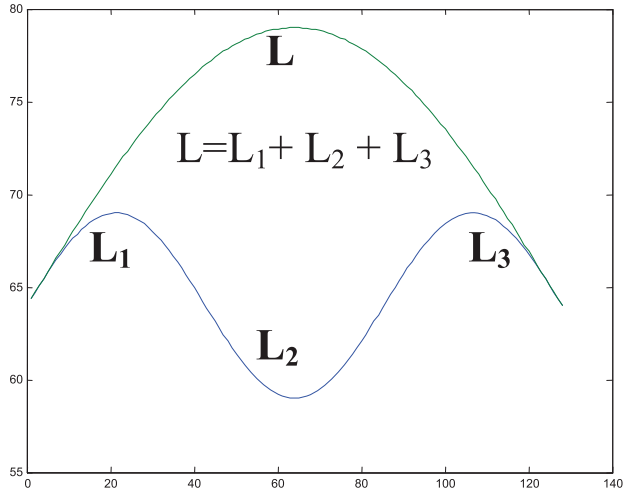

Fig. 1 The first and second curves (top and bottom) have same length, L and chord length, $C = 128$, but very different tortuosity.

is the ratio between its arc length and length of underlying chord (referred as L-C in the present work) [4], [5]. It gives a value of unity for straight line and increases with vessel elongation. This measure does not account for measuring morphology or hemodynamic consequences. Moreover, the surface of the retina is analogous to a circle arc with a large radius and is considered non-tortuous; thereby L-C measure is recognized as flawed. Besides it is shown in Fig. 1 that the measure fails in distinguishing two vessels with different tortuosity that have the same arc length over chord length measure.

2.2.2 Measures Involving Curvature

In the Euclidean plane, curvature is defined as the rate of change of slope as a function of arc length. Given a curve $y = f(x)$, the curvature at a point $p(x, y) \in R^2$ is expressed as,

$$\kappa(p) = \frac{d^2y/dx^2}{(1 + (dy/dx)^2)^{3/2}} \tag{6}$$

where dy/dx and d^2y/dx^2 are the first and second derivative respectively and $\kappa(p)$ is the curvature at the point, $p(x, y)$.

The above equation often produces errors in discrete curves. To calculate curvature at each point on curve, an index based on second difference of the coordinates of the vessel midline (referred as TC in this study) was proposed [10].The total curvature, TC, was measured by taking the sum of the difference in slope of two successive segments, (that is, difference in slope between the three successive points along the midline on the given vessel curve). However all these measures require arbitrary smoothing schemes to smooth the noise in the coordinates resulting from limited sampling. Moreover, if a tortuosity metric is to be useful in detecting and characterizing abnormal patterns of tortuosity, it should give high tortuosity values to curves with high frequency and high amplitudes, but results show this measure does not fulfill this criterion.

2.3 Proposed Tortuosity Measure

Our approach is based on principal component analysis (PCA) of the coordinates of the vessel midline. It is a popular primary technique in pattern recognition, dimensionality reduction and feature extraction. Among the true eigenvector-based multivariate analyses, PCA is the simplest technique that reveals the internal structure of the data in a way that best explains the variance in the data. PCA on simulated blood vessels provide a way to identify predominant curvature patterns. A mathematical procedure, PCA is implemented by eigenvalue decomposition of a data covariance matrix of each sub vessel (sub-segment) following whitening procedure (implies centering the data for each attribute). For the covariance matrix, the eigenvectors corresponds to the principal components and eigenvalues to the variance explained by the principal components. This operation ensures that the first principal component describes the direction of maximum variance. Eigenvectors are perpendicular to each other and provide information about the patterns in the data.

Eigenvalues provide quantitative assessment of how much a component represents the data. Higher eigenvalues of a component show that the representation of the data is more in terms of variance and is referred as the leading eigenvalue. Eigenvectors with highest eigenvalue is the principal component of the data set. It also represents the intensity of explained variance as a percentage of total variance. In our methodology, the eigenvalues of the covariance matrix determine the judge ment of practical significance. The factors with eigenvalues ratio close to zero, are considered practically insignificant, that is, as explaining only a negligible portion of variability in the direction of blood vessel, while eigenvalues ratio approaching 1.00 are considered practically significant as explaining a large amount of data variability.

We define our tortuosity coefficient, T, as the ratio of second leading eigenvalue, λ_2 associated with the second principal axis, to the leading eigenvalue, λ_1 corresponding to the first principal axis. We calculate tortuosity of the whole vascular structure by taking the average of the sum of tortuosity values of each sub-vessel.

$$T = \sum_{i=1}^{n} \lambda_{2i}/\lambda_{1i} \tag{7}$$

λ_1 and λ_2 shows the variance along the two axes and n is the total number of sub segments of the entire blood vessel network. The proposed measure is modelled using simulated curves. For straight vessels, the index approaches zero, as $\lambda_2 \approx 0$ even though $\lambda_1 \gg 0$, and increases as the vessel becomes more tortuous, that is the second leading eigenvalue increases more as compared to the leading eigenvalue of the covariance matrix and becomes closer to the leading eigenvalue of the covariance matrix ($\lambda_2 \approx \lambda_1$). Since our proposed index is based on ratio of eigenvalues,

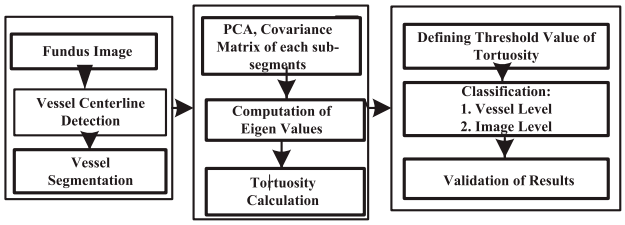

Fig. 2 Architecture of tortuosity measurement algorithms.

the associated computation is relatively simpler compared to other proposed indices and is dimensionless since both the numerator and denominator have the same dimensions. It satisfies the properties required for a valid tortuosity metric for retinal vessel evaluation.

We have not considered further other proposed measures of tortuosity, such as the number of inflection points and angle change along segments, since they performed poorly in an earlier study [17].

Figure 2 shows the system architecture at a glance for the proposed tortuosity index. The procedure is demonstrated into three successive blocks with the first block depicting the image preprocessing, the second block showing the tortuosity measurement process and the third block showing the classification of the retinal vessels and its validation against the judgement of expert ophthalmologists.

2.4 Experimental Procedure and Setup

To test the performance of the proposed tortuosity index and to compare it with other available indices, two types of experiments are performed. In the first one, different types of vessels are simulated (see Fig. 3) to evaluate the compliance of various methods with the tortuosity properties described in Sect. 2.1. Values for the four indices (TC, L-C, Grisan metric and the proposed index) are calculated for each case where TC is the tortuosity coefficient based on second differences of the coordinates of the vessel midline [10]; L-C is the traditional arc to chord length ratio and Grisan metric evaluated by integrating the number of turn curves and arc to chord length ratio. In the second experiment, vessel centerline of a set of retinal images from infant retina is extracted and segmented according to improved branching point and ending point detection technique and analyzed by the proposed approach. The results are verified against the judgement of two expert ophthalmologists.

2.4.1 Simulated Vessels

In order to test how the various proposed tortuosity measures vary when single parameters that influence the clinical perception of tortuosity changes, three sets of simulated vessels are generated as shown in Fig. 3.

The first set of simulated vessels is composed by a sequence of sinusoids with same frequency, f and chord length, C, but different amplitude, A where $A \in [5, 10, 15, 20, 25, 30, 35, 40]$, $C = 128$, $f = 1$ (Fig. 3 (a)).

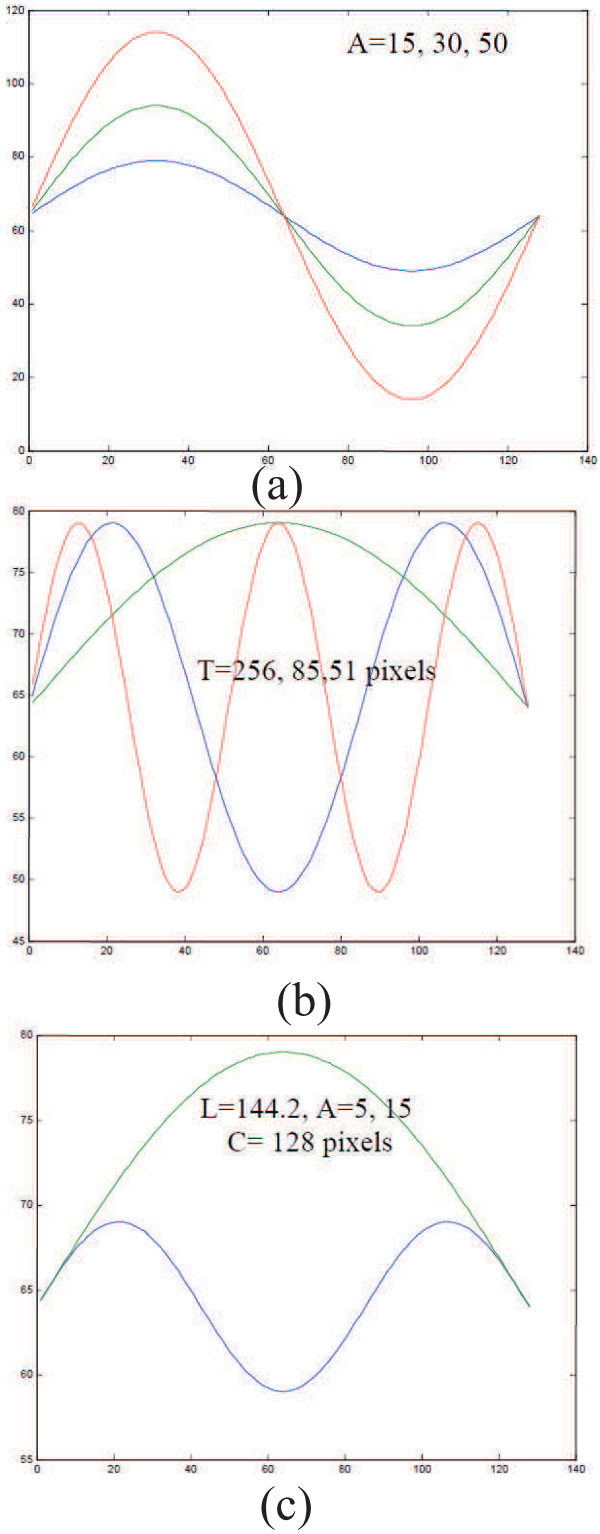

Fig. 3 Different types of simulated vessel. Note: In figure 3 (b) Values of T = 256, 85, 51 pixels is equivalent to f = 0.5, 1.5, 2.5

The second set is composed by a sequence of sinusoids with the same amplitude, A, and chord length, C, but different frequency, f where $A = 15$, $C = 128$, and $f \in [0.5, 1, 1.5, 2, 2.5, 3, 3.5, 4]$ (Fig. 3 (b)).

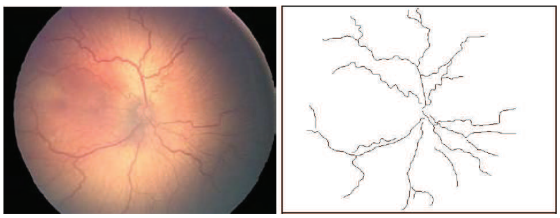

(a) (b)

Fig. 4 Left: The original image. Right: Detected vessel centerline.

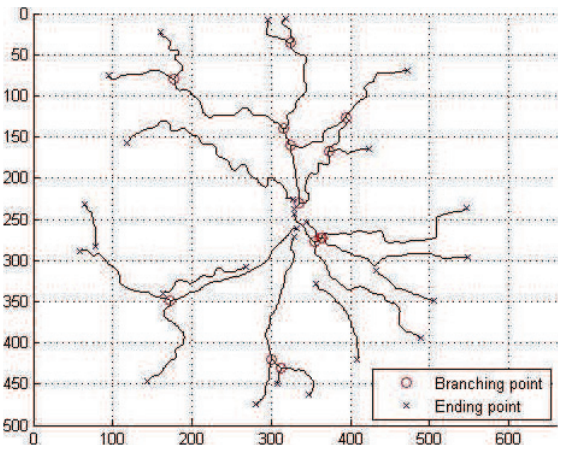

Fig. 5 Vessel segmentation by improved branching point and terminal point detection.

The third and the last set of simulated vessels is composed by a sequence of curves with constant curvature (in absolute value), but increasing number of changes in curvature sign. These curves are built such that they have the same chord length, C and arc length, L, but different amplitude and frequency (shapes), that is different curvature signs; however the absolute curvature remains the same. In this case, $A \in [15, 8.3, 5, 4, 3]$, $L = 144.42$, $C = 128$, absolute net curvature = 57 (Fig. 3 (c)). It is to be noted that only some of the simulated curves are shown in Fig. 3 (a)-(c).

2.4.2 Skeletonised Retinal Images

In the second part of the experiment, the proposed measure is tested on a set of 45 actual retinal images of infant retina. The extracted vessel centerline of ground truth retinal images (Images with hand-labeled blood vessel network under supervision of expert clinicians shown in (Fig. 4)) are segmented by branching point and ending point (Fig. 5). These 45 images are segmented into 1676 sub segments. They are divided into training set and test set. The proposed approach is applied to each sub vessel sample and tortuosity is calculated as in Eq. (7).

2.4.3 Improved Branching and Terminal Nodes Detection

Terminal and branching points are detected using the skeleton image. We track every vessel pixel and count the number, n, of pixel around the eight neighborhood of a current

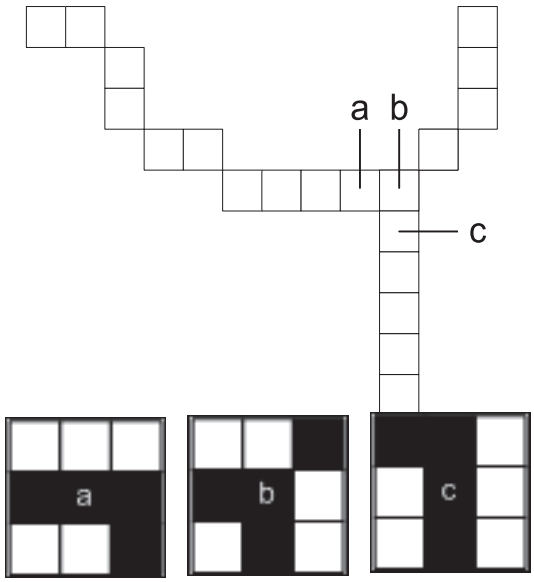

Fig. 6 A vessel segment of a digital curve.

location that has the same intensity as vessel pixel, and use this number to classify the point as ending point ($n = 1$), non-significant point ($n = 2$) and candidate for branching point ($n \geq 3$).

In [18], Trucco et al defined branching point as n more than or equal to 3. We found that sometimes it gives wrong results. For example, the value of n corresponding to the point a, b and c in Fig. 6 is 3 which is considered as a branching point by definition of [18]. Based on early observations, to get actual branching point, this time we compute the four connectivity of the branching point candidate by ignoring other branching point candidates. If there is no connectivity in each eight neighborhood, that branching point candidate is marked as a branching point. In this case only point b should be considered as a branching point.

2.5 Classification

Classifications are performed at 2 levels. The first level is vessel level. In order to classify the retinal vessels into two classes of tortuous and non- tortuous vessels, we adopt a classification scheme. To facilitate comparison with previous work, the classifier we used is Naive Bayes classifier. We give a short review of the Bayesian model here and refer the reader to [19], [20] for details. The Naive Bayes classifier is the probabilistic classifier based on applying Bayes' theorem. The following equation is the Bayes rule used in Naive Bayes classification.

$$P(y|x) = \frac{P(x|y)P(y)}{P(x)} \tag{8}$$

The Naive Bayes classifier uses the principle of Bayesian Maximum a Posteriori (MAP) classification: measure the feature data then select the class.

$$\hat{y} = \underset{y}{\operatorname{argmax}}\ P(y|x) \tag{9}$$

Table 1 Breakdown of ground truth database.

	Tortuous	Non-Tortuous
Expert 1	186	314
	5	43
Expert 2	194	306
	4	44
Agreed Result	173	309
	4	41
Train Data	119	207
	2	28
Test Data	54	102
	2	13

$P(y|x)$ is the parameter we want to estimate. It is the hypothesis y and a finite set of features x which bears on the hypothesis. $P(x|y)$ is the likelihood of feature x given class y, $P(x)$ is an independent probability of feature x and $P(y)$ is the priori probability of class y. The equation below is the Bayes rule used in Naive Bayes classifier.

$$P(tortuous\ class|tortuousity\ value) = \frac{P(tortuosity\ value|tortuous\ class)P(tortuous\ class)}{P(tortuosity\ value)} \tag{10}$$

$$tortuous\ class = tortuous, non\text{-}tortuous$$

Naive Bayes assumes that the features are conditionally independent given a class. We estimate the parameters $P(x|y)$ and $P(y)$ from training data.

For the first classification problem, two expert ophthalmologists were asked to classify each segment of vessel from vessel tree as tortuous or non-tortuous. They labelled 500 randomly selected sub vessel samples from the set of forty five images out of which only 482 sub vessels (agreed results) were used for analysis. The ophthalmologists were also asked to grade each image as tortuous or non-tortuous by looking at the whole vessel tree as one structure for the second level that is frame level or image level analysis. The grading of the experts are based solely on their experiences. Table 1 shows the breakdown of ground truth database at sub vessel level (first row) and Image level (second row). Only the agreed results from both the experts, are used as a ground truth in the training and testing phase. 67.5% of the data were used to train the classifier at sub vessel level and a training set of 30 images for Image-level analysis. We evaluate performance on test set quantitatively by comparing the classifier's result to ground truth. The mean classification rate on the testing subsets were used to evaluate the performance of the classifier. The classification rate gives the overall success rate of the classifier for each metric.

All of the 45 images were converted to binary form for implementation.

3. Results and Discussion

The Fig. 7 shows, our PCA-based proposed index as applied to each sub vessels. The line along a sub vessel curve is the principal axis and the 'cross' sign denotes the data point

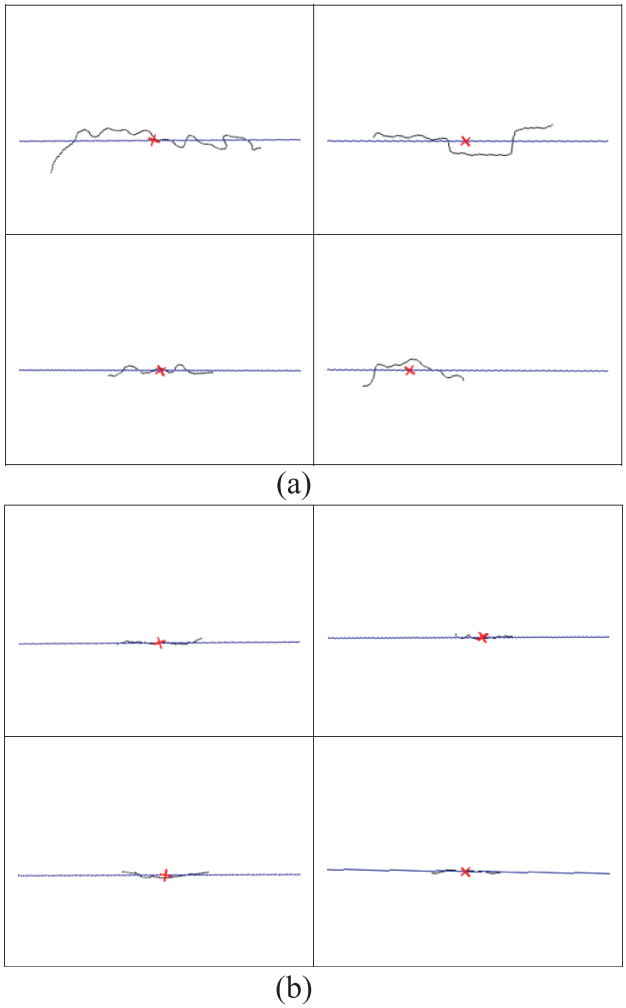

Fig. 7 (a) Tortuous vessels. *Note: Proposed index, T = 0.0346, 0.0456, 0.0253, 0.0124, starting from top left in clockwise direction* (b) Normal (non tortuous) vessels. *Note: Proposed index, T = 0.0031, 0.0046, 0.0058, 0.0078, starting from top left in clockwise direction*

of mean of the x and y coordinates of the sub vessel and therefore it is shifted for each sub vessel curve depending upon its respective x and y coordinates' values (or in other words, the cross sign denotes the sample mean, it locates the centre of gravity of the cloud of points formed by the data samples in d-dimensional space). The horizontal axis is the first principal axis, where the variance is greatest and represents the position or distance along the vessel (the leading eigenvalue). The vertical axis is the second principal axis, where the remaining variance is greatest, and it represents the deviation from the horizontal axis and values of the second leading eigenvalue. It is observed that as the sub vessels becomes tortuous or curved, the index value increases as the second leading eigenvalue increases as compared to the leading eigenvalue or approaches the leading eigenvalue ($\lambda_2 \approx \lambda_1$, see Fig. 7 (a)). On the other hand, the value of the proposed index approaches zero, for almost straight sub vessels as $\lambda_2 \approx 0$ even though $\lambda_1 \gg 0$ (see Fig. 7 (b)). For straight vessels, $\lambda_1 > 0$, but $\lambda_2 = 0$. The principal axis fits

well for such straight sub vessels.

The results of simulated vessels are shown in Fig. 8 - Fig. 11, for the four indices.

In Fig. 8, the tortuosity measure, L-C as function of amplitude and frequency is shown. As both the sinusoid amplitude and frequency changes, a valid tortuosity measure is expected to increase with increasing amplitude and frequency. This proves that L-C satisfies the modulation property.

Figure 9 shows the tortuosity index, TC for varying values of amplitude and frequency. It is found that the index reaches its peak at A=25 for f=0.5 and then decreases. At f=1 and f=1.5, it reaches the maximum at A=10, then descends. After that as the frequency is increased from f=2 to f=4, it decreases for all values, as the amplitude is increased. That is to say, it follows the reverse of the expected trend, thereby shows that it does not satisfies the modulation property.

Figure 10 shows the tortuosity index, Grisan Metric for varying values of amplitude and frequency. It is observed that the index varies almost proportionally to amplitude and frequency changes as expected for a valid tortuosity index, therefore fulfills modulation property.

In Fig. 11, the proposed tortuosity measure, based on PCA as function of amplitude and frequency is shown. Table 2 displays values of proposed index for different frequency and amplitude values. For fixed frequency values, (e.g. $f = 1$) as the amplitude is increased in steps of five starting from amplitude equal to 5 to a maximum of amplitude value equal to 40, the values of the proposed measure increases, indicating that it fulfills the criterion of amplitude

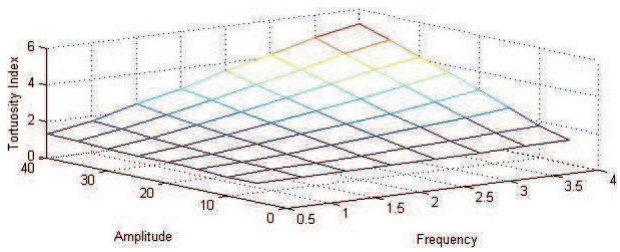

Fig. 8 3D Plot of L-C ratio for varying amplitude and frequency values.

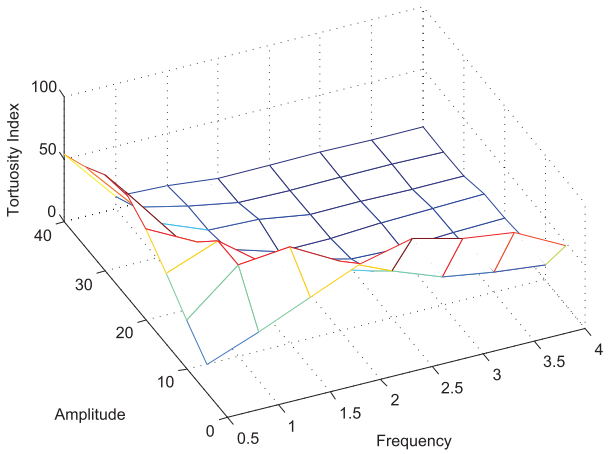

Fig. 9 3D Plot of total curvature, TC, for varying amplitude and frequency values.

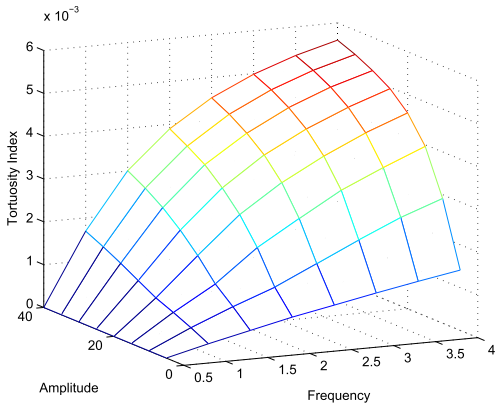

Fig. 10 3D Plot of Grisan Metric, for varying amplitude and frequency values.

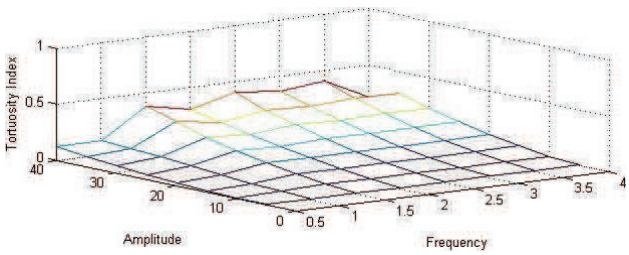

Fig. 11 3D Plot of proposed index, for varying amplitude and frequency values.

Table 2 Shows values of proposed index, T, based on PCA for varying Amplitude (vertically) and frequency (horizontally) where T= λ_2/λ_1.

Amplitude \ Frequency	0.5	1	1.5	2	2.5	3	3.5	4
5	0.0019	0.0038	0.0086	0.008	0.0091	0.0089	0.0093	0.0096
10	0.0072	0.0141	0.0335	0.0313	0.0339	0.0302	0.0308	0.0282
15	0.0159	0.0296	0.0755	0.0613	0.0678	0.0621	0.0632	0.0606
20	0.0283	0.0478	0.1199	0.0999	0.109	0.1005	0.1053	0.1047
25	0.0438	0.0697	0.1748	0.1418	0.1649	0.1534	0.1609	0.1602
30	0.0628	0.0898	0.2322	0.1948	0.2305	0.2122	0.23	0.2132
35	0.0849	0.1069	0.3126	0.2419	0.3042	0.2831	0.3079	0.2875
40	0.1108	0.1233	0.3886	0.3003	0.3975	0.3597	0.4017	0.3704

modulation. For the case of frequency modulation, the index increases as the value of frequency is increased until $f = 1.5$, then descends for $f = 2$, showing somewhat abrupt changes between $f = 2$ and $f = 3$, thereafter follows the expected trend. Therefore it is inferred that as both the sinusoid amplitude and frequency changes, the proposed tortuosity measure increases, though not proportionately, showing the maximum value at $A = 40$ and $f = 3.5$. This shows that the index is effective in detecting abnormal patterns of low frequency and large amplitude, and it does to an extent satisfy the modulation property. Since ROP falls under Type 1 abnormality where the normally straight or gently curved vessels begin to exhibit a more sinuous curve of relatively low frequency and large amplitude, the proposed index proves viable to detect phenomenal changes in such images.

A special case of flipped sinusoids (Fig. 12) is also tested on the four indices and found that L-C ratio cannot differentiate any changes, because it depends on the total curve length; however Grisan metric and TC could differentiate as the sinusoids are flipped from 0.7 to 0.5. i.e., follows the desired trend (the values of the index should increase as the sinosoids are flipped more.) Table 3 gives the values of the four indices. On the other hand, The proposed index, PCA is sensitive to such changes, although it actually decreases slightly as the sinosoids are flipped more. This is attributed to the fact that as the sinusoids are flipped more, the value of the second leading eigen value, λ_2 decreases whereas the value of the leading eigen value, λ_1 remains constant, as a result the value of the proposed index decreases since it is the ratio of the two eigen values.

Our point in this study is to prove whether our proposed measure, based on PCA is sensitive to the morphology of the vessel that is to the shape of its path in space irrespective of the point whether the observed appreciable changes (Table 3), are in the reverse fashion (Fig. 12). On the contrary, L-C ratio remains almost constant, consequently is insensitive to such changes. Therefore, in our pursuit to show the merits of the proposed measure over L-C metric, our proposed index, T, proved superior in some cases to the most simple and prevailing index, L-C.

Any useful tortuosity index should be independent of scale, so that a magnified image of a certain shape should have almost the same tortuosity value as the original. Table 4 shows the values of the four indices for different scales. It is observed that minor changes occur in the values of all the indices, but they lie in the permissible error range. Hence, it is concluded that the proposed index along with TC and L-C does fulfill this important criterion of scale-independence. On the other hand, Grisan Metric fails to satisfy this pre-requisite since it is not a dimensionless index.

An ideal tortuosity index should vary inversely to chord length. Table 5 shows values of the tortuosity indices calculated for $1/2$ sinusoid of different chord lengths and amplitude fixed as $A = 15$. As the chord length increases, and the sinusoid becomes less curved, the indices become smaller as expected.

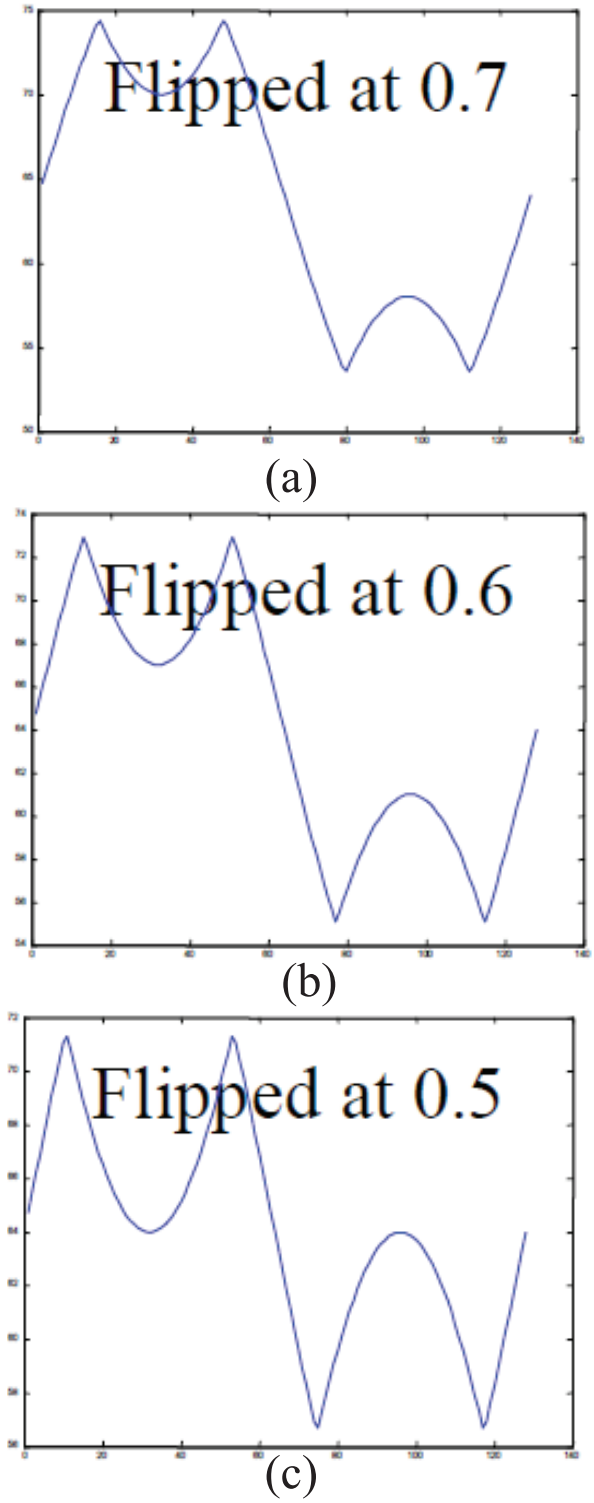

Fig. 12 Flipped Sine wave at 0.7, 0.6 and 0.5.

A tortuosity index useful in detecting and characterizing abnormal patterns of tortuosity should be sensitive to curves with high frequency but low amplitude (see Fig. 3 (c)). Results in Table 6 show that Grisan metric does fulfill this criterion, whereas L-C and TC theoretically remains constant. Juxtaposed our proposed measure shows

changes, although the values of the index actually decrease for low amplitude and high frequency curves, signifying that it is not sensitive to small ripples that perhaps be seen in blood vessels due to artifacts or noise. Notwithstanding, it works well for our experimental set-up composed of infant retinal images, that are characterized by low frequency, large amplitude blood vessels (Type 1 abnormality).

Table 7 compares the properties of our proposed measure based on PCA with three other previously proposed indices. The L-C ratio commonly used as an index of tortuosity only indicates vessel elongation and has no value in measuring morphology or hemodynamic consequences. The rationale of TC is unclear for modulation property. Grisan Metric shows scale variance. Our PCA based index behaves consistently with intuitive notions of tortuosity. It represents analogs of L-C measure, except that the latter was not defined in terms of standard deviation along the orthogonal axis and cannot differentiate between different shapes.

Table 3 Values of indices for shapes shown in Fig. 12.

	L-C	Proposed index	TC	Grisan Metric
Sine wave	1.1924	0.0297	73	0.0008
Sinewave, flipped at 0.7	1.1793	0.0121	65	0.0005
Sinewave, flipped at 0.6	1.1793	0.0076	69	0.0006
Sinewave, flipped at 0.5	1.1793	0.0055	73	0.0009

Table 4 Values of the indices for different scales.

	L-C	Proposed index	TC	Grisan Metric
A=15, Chord Length, L = 128	1.1924	0.0297	73	0.0006
A=30, Chord Length, L = 256	1.1933	0.0293	77	0.0003
A=60, Chord Length, L = 512	1.1937	0.0292	78	0.0001

Table 5 Values of the indices for sinusoid of different lengths.

Length	L-C	Proposed index	TC	Grisan Metric
128	1.1363	0.0171	57	0.0005
256	1.0487	0.0039	28	0.0002
512	1.0259	0.0009	24	0.0001

Table 6 Values of the indices for of different twists.

Frequency	Amplitude	L-C	Proposed index	TC	Grisan Metric
0.5	15	1.1363	0.0171	57	0.0000
1.0	8.3	1.1382	0.0109	57	0.0004
1.5	5	1.1363	0.0080	57	0.0006
2.0	4	1.1382	0.0054	57	0.0007
2.5	3	1.1363	0.0032	57	0.0008

3.1 Model Verification

We compared results of our proposed measure at segment level with three metrics reported earlier in literature: the L-C, TC, and the metric suggested by Grisan et al. Confusion matrices are used and experiments are conducted with our own implementations of various measures. In our confusion matrices, each column gives the percentages of the vessels classified by the system in this row (for e.g., tortuous) that were classified in each class (tortuous and non- tortuous) by the clinicians. Therefore, the entries of each column adds to 100, but the rows do not need to.

For Grisan's method we used the threshold value of 0.015 (average of 0.03 for arteries and 0.01 for veins considered in [13]).

Table 8 shows the confusion matrices comparing automatic classification against clinical judgement. We show results for L-C, TC, Grisan's metric and our proposed measure. Table 9 shows the classification accuracy of the corresponding metrics. This Table reports the classification rates at segment level and image level. The classification rate is simply the proportion of test samples that are correctly classified.

In this study, we examined retrospectively the retinal fundus images of infants both normal and pathological and computed values of the tortuosity metric for each retinal vessels within an image. The tortuosity values are validated against agreed results of two expert ophthalmologists. We

Table 7 A comparison of the tortuosity indices with respect to the required properties (-do- indicates that an index shows the required property; X that it does not).

Properties	L-C	TC	Grisan Metric	Proposed index
Scaling	-do-	-do-	X	-do-
Modulation	-do-	X	-do-	-do-
Shape	X	-do-	-do-	-do-
Length	-do-	-do-	-do-	-do-
Additive	X	-do-	-do-	X

Table 8 Classification performance as confusion matrices.

	Classify result \ Ground truth	Tortuous Vessel	Non-Tortuous Vessel
Arc-chord Ratio	Tortuous Vessel	64.81 (35)	30.39 (31)
	Non-Tortuous Vessel	35.18 (19)	69.61 (71)
TC	Tortuous Vessel	64.81 (35)	48.04 (49)
	Non-Tortuous Vessel	35.18 (19)	51.96 (53)
Grisan Metric	Tortuous Vessel	59.25 (32)	27.45 (28)
	Non-Tortuous Vessel	40.74 (22)	72.55 (74)
Proposed index,T	Tortuous Vessel	79.62 (43)	13.73 (14)
	Non-Tortuous Vessel	20.38 (11)	86.27 (88)

Table 9 Classification accuracy of different tortuosity measures.

Tortuosity Index	Arc-chord Ratio	TC	Grisan Metric	Proposed index, T
Classn Rate (Segment)	67.21	58.39	65.89	82.94
Classn Rate (Image)	73.33 (11)	53.33 (08)	66.67 (10)	86.66 (13)

Note: The values in parentheses in the above two tables gives the number of correctly classified test samples

wished to test whether our tortuosity index can successfully mimic the judgment of human experts. The best set of parameters produced 82.94% and 86.6% classification rate at vessel segment level and image level respectively.

Our method predominates the conventional L-C index, as it could differentiate between different shapes (flipped case) and those having same arc length but different number of twists (refer Fig. 3 (c) and Table 6).Evaluation of the tortuosity measure was done on ground truth retinal vessels to avoid possible errors and variability arising from the different automatic vessel tracing procedures available.

4. Conclusion

We investigate our tortuosity measure by analyzing abstract properties of metrics based on medical intuitions of tortuosity. Classification is carried out in two tiers to categorize blood vessel segments and blood vessel networks, in order to evaluate the integrity of the proposed measure. An improved approach of splitting the network of blood vessels into sub vessels is proposed, and it is characterized by branching and terminal point detection.

An attempt is made to quantify the morphological features of the full micro vascular network in the retina by taking the mean of the values of the tortuosity index measured using each of the vessels within the images. The numerical experiments show the efficiency and robustness of the proposed index as applied to 45 medical images of the retina. The index may be useful in selecting infants with Plus disease, one of the most important prognostic indicators in ROP. However, the clinical definition of abnormal tortuosity can vary from disease to disease [7]; therefore, extensive testing on a large number of infants with vessels ranging widely in tortuosity is needed to further validate the index. The tortuosity values that have been computed thus far apply to vessel segments. Current work aims at generalizing this treatment, in order to characterize a network of branched vessels, such as occur in the micro vascular network of the retina. An earlier attempt to this [21], (analogous to our approach) also used the average tortuosity of vessel segments to characterize such a network. Investigations are underway to assess the goodness of the proposed measure in other retinopathies having similar vascular morphology changes, such as diabetic retinopathy, hypertensive retinopathy and cardiovascular diseases.

Acknowledgements

The authors are grateful to Thammasat eye Centre for providing the necessary support and to Dr. Sakchai V. and Dr. Nattapol W. for grading the images segment wise. This project is funded by National Research University Project of Thailand Office of Higher Education Commission.

References

[1] T.Y. Wong, R. Klein, D.J. Couper, L.S. Cooper, W. Shahar, L.D. Hubbard, M.R. Wofford, and A.R. Sharret, "Retinal microvasculature abnormalities and incident stroke: The atherosclerosis risk in communities study," The Lancet, vol.358, pp.1134–1140, 2001.

[2] J.J. Capowski, J.A. Kylstra, and S.F. Freedman, "A numeric index based on spatial frequency for the tortuosity of retinal vessels and its application to plus disease in retinopathy of prematurity," Retina, vol.15, no.6, pp.490–500, 1995.

[3] T. Aslam, B. Fleck, N. Patton, M. Trucco, and H. Azegrouz, "Digital image analysis of plus disease in retinopathy of prematurity," Acta Ophthalmol, vol.87, pp.368–377, 2009.

[4] W. Lotmar, A. Freiburghaus, and D. Bracher, "Measurement of vessel tortuosity on fundus photographs," Graefes Archive for Clinical and Experimental Ophthalmology, vol.211, pp.49–57, 1979.

[5] D. Bracher, "Changes in peripapillary tortuosity of the central retinal arteries in new borns," Graefes Archive for Clinical and Experimental Ophthalmology, vol.218, no.4, pp.211–217, 1982.

[6] W.E. Hart, M. Goldbaum, B. Cote, P. Kube, and M.R. Nelson, "Automated measurement of retinal vascular tortuosity," Int. J. Medical Informatics, vol.56, pp.239–252, 1999.

[7] E. Bullit, G. Gerig, S. Pizer, W. Lin, and S. Aylward, "Measuring tortuosity of the intracerebral vasculature from mra images," IEEE Trans. Med. Imaging, vol.22, no.9, pp.1163–1171, 2003.

[8] J.A. Kylstra, T. Wierzbicki, M.L. Wolbarst, M.B. Landers, and E. Steffansson, "The relationship betweem retinal vessel tortuosity, diameter and transmural pressure," Graefes Archive for Clinical and Experimental Ophthalmology, vol.224, pp.477–480, 1986.

[9] A. Kaupp, H. Toonen, S. Wolf, K. Schulte, R. Effert, D. Meyer-Ebrecht, and M. Reim, "Automatic evaluation of retinal vessel width and tortuosity in digital flourescein angiograms," Investigative Ophthalmology & Visual Science, vol.32, p.952, 1991.

[10] G. Dougherty and J. Varro, "A quantitative index for the measurement of the tortuosity of blood vessels," Medical Engineering & Physics, vol.22, pp.567–574, 2000.

[11] X.W. Gao, A. Bharath, A. Stanton, A. Hughes, N. Chapman, and S. Thom, "Quantification and characterisation of arteries in retinal images," Computer Methods and Programs in Biomedicine, vol.63, pp.133–146, 2000.

[12] L. Pedersen, M. Grunkin, B. Ersbull, K. Madsen, M. Larsen, N. Christoffersen, and U. Skands, "Quantitative measurement of changes in retinal vessel diameter in ocular fundus images," Pattern Recognit. Lett., vol.21, pp.1215–1223, 2000.

[13] E. Grisan, M. Foracchia, and A. Ruggeri, "A novel method for the automatic grading of retinal vessel tortuosity," IEEE Trans. Med. Imaging, vol.27, no.3, pp.310–319, 2008.

[14] C. Heneghan, J. Flynn, M.O. Keefe, and M. Cahill, "Characterization of changes in blood vessel width and tortuosity in retinopathy of prematurity using image analysis," Medical Image Analysis, vol.6, pp.407–429, 2000.

[15] L. Sukkaew, B. Uyyanonvara, S.S. Makhanov, S. Barman, and P. Pangputhipong, "Automatic tortuosity- based retinopathy of prematurity screening system," IEICE Trans. Inf. & Syst., vol.E91-D, no.12, pp.2868–2874, Dec. 2008.

[16] M.J. Johnson and G. Dougherty, "Robust measures of three-

dimensional vascular tortuosity based on the minimum curvature of approximating polynomial spline fits to the vessel mid-line," Med Eng Phys, vol.29, pp.677–690, 2007.
[17] O. Smedby, N. Hogman, S. Nilsson, U. Erikson, A.G. Olsson, and G. Walldius, "Two-dimentional tortuosity of the superficial femoral artery in early atherosclerosis," J. Vasc Res, vol.30, pp.181–191, 1993.
[18] E. Trucco, H. Azegrouz, and B. Dhillon, "Modelling the tortuosity of retinal vessels: Does calibre play a role?," IEEE Trans. Biomed. Eng., vol.57, no.9, pp.2239–2247, 2010.
[19] N. Friedman, D. Geiger, and M. Goldszmidt, "Bayesian network classifiers," Machine Learn., vol.29, pp.131–163, 1997.
[20] D.D. Richard, E.H. Peter, and G.S. David, Pattern Classification second edition, pp.20–83, A Wiley-Interscience Publication, 2000.
[21] S.B. Bidiwala, M.S. Mansour, C.K. Stengel, S.A. Klein, and S.M. Carroll, "Quantification of the morphological features of a full microvascular network," Med Biol Eng Comput, vol.36, pp.621–626, 1998.

Rashmi Turior received her M.tech in Biomedical Engineering from Manipal Institute of Technology, Manipal, India in 2004 and her B.E. in Electrical & Electronics from DSCE, Bangalore University, Bangalore, India in 1998. She is currently a Ph.D. student in the School of Information and Computer Technology at Sirindhorn International Institute of Technology, Thammasat University, Thailand. She is also Assistant Professor (on leave) in the Department of Electronics and Telecommunication at JSCOE, Pune University, India, where she has been faculty since January 2005. Her research areas include Retinal imaging and Biomedical signal processing and image processing.

Danu Onkaew received his Bachelors in Computer Engineering and is currently a Master degree student at Sirindhorn International Institute of Technology, Thammasat University, Thailand. His research areas include Retinal imaging and image processing.

Bunyarit Uyyanonvara received his Ph.D. in Image Processing, King's College, University of London, UK and B.Sc. (1st Class Honors) in Science (Physics), Prince of Songkhla University, Thailand. He is now an Associate Professor at Sirindhorn International Institute of Technology, Thammasat University, Thailand. His research areas include Medical image analysis and Pattern recognition